HHS Public Access

Author manuscript

Nat Cell Biol. Author manuscript; available in PMC 2016 November 23.

Published in final edited form as:

Nat Cell Biol. 2016 July ; 18(7): 752–764. doi:10.1038/ncb3363.

The Polycystin complex mediates WNT/Ca^{2+} signaling

Seokho Kim[#1], **Hongguang Nie**[#1,4], **Vasyl Nesin**[1], **Uyen Tran**[2], **Patricia Outeda**[3], **Chang-Xi Bai**[1,5], **Jacob Keeling**[1], **Dipak Maskey**[1], **Terry Watnick**[3], **Oliver Wessely**[2], and **Leonidas Tsiokas**[1,7]

[1]Department of Cell Biology, University of Oklahoma Health Sciences Center, 975 NE 10th Street, Oklahoma City, OK 73104, USA

[2]Department of Cellular and Molecular Medicine, Cleveland Clinic, 9500 Euclid Avenue/NC10, Cleveland, OH 44195, USA

[3]Division of Nephrology, Baltimore PKD Research and Clinical Core Center, University of Maryland School of Medicine, 655 West Baltimore Street, Baltimore, MD 21201, USA

[4]Institute of Metabolic Disease Research and Drug Development, China Medical University, Liaoning Shenyang, 110001 China (H.N)

[5]Department of Advanced Research on Mongolian Medicine, Research Institute for Mongolian Medicine, Inner Mongolia Medical University, Hohhot 010110, Inner Mongolia, China (CB)

[#] These authors contributed equally to this work.

Abstract

WNT ligands induce Ca^{2+} signaling on target cells. PKD1 (Polycystin 1) is considered an orphan, atypical G protein coupled receptor complexed with TRPP2 (Polycystin 2 or PKD2), a Ca^{2+}-permeable ion channel. Inactivating mutations in their genes cause autosomal dominant polycystic kidney disease (ADPKD), one of the most common genetic diseases. Here, we show that WNTs bind to the extracellular domain of PKD1 and induce whole cell currents and Ca^{2+} influx dependent on TRPP2. Pathogenic *PKD1* or *PKD2* mutations that abrogate complex formation, compromise cell surface expression of PKD1, or reduce TRPP2 channel activity suppress activation by WNTs. *Pkd2*$^{-/-}$ fibroblasts lack WNT-induced Ca^{2+} currents and are unable to polarize during directed cell migration. In *Xenopus* embryos, PKD1, Dishevelled 2 (DVL2), and WNT9A act within the same pathway to preserve normal tubulogenesis. These data define PKD1

[7]Correspondence should be addressed to L.T. (ltsiokas@ouhs.edu).

AUTHOR CONTRIBUTIONS

S.K. performed protein-protein interaction and cell migration assays; H.N and V.N. performed electrophysiological experiments; U.T and O. W. performed experiments in *Xenopus* embryos; P.O. and T. W. provided mouse embryonic fibroblasts from wild type and *Pkd1*- and *Pkd2*-null mice; C. B. performed Ca^{2+} imaging experiments; J.K. and D. M. analyzed expression profile of FZDs, DVLs, and other WNT (co)receptors in wild type and *Pkd2*-null cells. L.T. supervised the study, analyzed data and wrote the paper with the help of S.K. and H.N. S.K. and H.N. contributed equally to the study. All authors discussed the results and commended on the manuscript.

COMPETING FINANCIAL INTERESTS

The authors declare no competing financial interests.

Supplementary Information is available in the online version of the paper

as a WNT (co)receptor and implicate defective WNT/Ca^{2+} signaling as one of the causes of ADPKD.

Introduction

The WNT signaling pathway regulates essential biological functions[1-3]. It is divided into two major arms, the canonical WNT/β-catenin pathway, and a β-catenin independent pathway that is mainly responsible for establishing planar cell polarity (PCP) and tissue morphogenesis. Activation of the noncanonical pathway is often accompanied by a transient increase in intracellular Ca^{2+} ($[Ca^{2+}]_i$)[4]. The pathway leading to this increase in $[Ca^{2+}]_i$ is poorly defined, but it seems to involve Ca^{2+} release from intracellular stores downstream of the activation of Frizzled (FZD)[5-7] and RYK receptors[8]. There is also evidence for WNT-induced Ca^{2+} influx, probably through transient receptor potential (TRP) or store-operated Ca^{2+} channels[7, 9]. However, specific receptors and channels responsible for WNT-induced Ca^{2+} influx are unknown.

In the mouse embryonic kidney, tubular diameter is controlled by WNT9B in a β-catenin independent manner[10]. A similar mechanism seemed possible for PKD1[11, 12], suggesting that WNT9B and PKD1 may function in the same pathway. PKD1 is a large protein of unknown function [13] (Fig. 1a). Its extracellular portion contains two leucine rich repeats (LRR) flanked by N- and C-terminal cysteine-rich domains (CRDs) followed by a cell-wall integrity and stress response component (WSC) domain. A second CRD showing weak homology to low density lipoproteins (LDL-A domain) is located downstream (Fig. 1a)[14]. These domains are unique to PKD1 and not present in homologous molecules such as PKD1L1-3. The C-terminal cytoplasmic tail of PKD1 interacts with multiple G protein α-subunits[15] and TRPP2[16-18]. TRPP2 belongs to the transient receptor potential (TRP) superfamily of ion channels and forms a Ca^{2+}-permeable non-selective cation channel in association with PKD1[19, 20] or other TRP channels[20-23]. The structure of PKD1 along with its ability to associate with TRPP2 has suggested that PKD1 and TRPP2 form a receptor/channel complex. However, the molecular identity of the ligand(s) of this complex and thus, its physiological mechanism of activation has been a mystery.

In this study, we identify secreted WNTs as activating ligands of the PKD1/TRPP2 complex. Activation of PKD1/TRPP2 by WNTs is independent of FZD receptors. We further show that TRPP2 is required for WNT9B-induced directed cell migration, a Ca^{2+}-dependent process often used as a surrogate assay for morphogenetic cell movements (convergent extension) during kidney tubule elongation. Finally, we identify DVL2 as an interacting partner of PKD1 and show that WNT9A, PKD1, and DVL2 function in the same pathway to control *Xenopus* pronephric tubule formation.

Results

WNT ligands can bind to the extracellular domain of PKD1

The cystic phenotype of *Wnt9b*-kidney null mice, along with the presence of several CRDs in PKD1 prompted us to test whether WNTs could physically interact with PKD1. Indeed,

WNT9B co-immunoprecipitated with PKD1 but not with the structurally similar PKD1L1 or TRPC1 (Fig. 1b). Next, we tested whether WNT9B could associate with various fragments of the extracellular domain unique to PKD1 in the extracellular space. The CRD of FZD8 was used as a reference point, since its affinity to WNT9B is known (K_D=482±16 nM[24]). WNT9B associated with the LRR-WSC-Fc and LDL-A-Fc (Fig. 1c). LRR-WSC-Fc also associated with WNT9B in the extracellular space *in trans*, whereby cells were singly transfected with Fc constructs or WNT9B, co-cultured for 24 h, and protein-protein interactions were detected in the cultured media (Fig. 1d). PKD1 interacted with WNT9B through a site that included the C-terminal CRD of the LRR and the WSC domain (LRR-CT +WSC-Fc, Fig. 1e). To test whether PKD1 and WNT9B interacted directly, we purified LRR-WSC-Fc from conditioned media of stably transfected HEK293 cells and incubated it with purified WNT9B. 87 ng (or 2.35 pmol) of purified WNT9B was pulled-down with 390 ng (or 5.2 pmol) of purified PKD1-Fc fusion (Fig.1f-h). Under the same conditions, full-length TRPP2-Myc isolated from total cell lysates did not interact with purified WNT9B (Supplementary Fig. 1g).

WNT5A, WNT4, or WNT3A also bound to LRR-WSC (Supplementary Fig. 1). WNT5A and WNT4 bound also to the LDL-A domain of PKD1 (Supplementary Fig. 1b-e). The affinity of WNT3A to soluble FZD8-CRD is 3.6±1.2 nM[24]. Thus, using the FZD8-CRD/WNT9B and FZD8-CRD/WNT3A interactions as “affinity rulers”, we deduced that the PKD1/WNT9B or PKD1/WNT3A interactions were of comparable affinity to that of FZD8/WNT3A. Therefore, PKD1 can interact with WNTs that function through β-catenin (WNT3A), independently of β-catenin (WNT5A), or both (WNT9B, WNT4), with an estimated affinity in the low nanomolar range.

WNT9B activates heterologously expressed PKD1/TRPP2 complex

Next, we tested whether CHO-K1 cells co-transfected with PKD1 and TRPP2 could support an increase in $[Ca^{2+}]_i$ in response to WNT9B. CHO-K1 cells do not express endogenous PKD1 or TRPP2[19]. Perfusion of untransfected cells with purified WNT9B did not result in an increase in $[Ca^{2+}]_i$ (Fig. 2a). In contrast, WNT9B induced an increase in $[Ca^{2+}]_i$, only in the presence of extracellular Ca^{2+} in cells co-transfected with PKD1 and TRPP2 (Fig. 2b,c). These data indicated that PKD1 and TRPP2 mediated WNT9B-induced Ca^{2+} influx rather than Ca^{2+} release from intracellular stores.

WNT9B-induced whole cell currents were determined in 50 nM intracellular Ca^{2+} using the whole cell configuration of the patch clamp technique. Addition of WNT9B (500 ng/ml) induced large currents in cells co-transfected with wild type PKD1 and TRPP2 (Fig. 2d,e). These currents were ~50-100-fold larger than PKD1/TRPP2 currents reported earlier[19, 25, 26]. Cells co-transfected with the pathogenic $PKD1^{S99I}$ [27] and TRPP2 failed to respond to WNT9B (Fig. 2f,i,l), although $PKD1^{S99I}$ was expressed at comparable levels to wild type PKD1 (Supplementary Figs. 2a and 3a). Cell surface biotinylation revealed that S99I severely compromised surface expression of $PKD1^{S99I}$ (Supplementary Fig. 2b). However, cell surface expression of TRPP2 was unaffected (Supplementary Fig. 2c). Consistently, cell surface expression of TRPP2 was unchanged in wild type and *Pkd1*-null

mouse embryonic fibroblasts (MEFs) (Supplementary Fig. 2d). These data suggested that cell surface expression of PKD1 is required for WNT9B-induced currents.

Because at 50 nM of intracellular Ca^{2+} other Ca^{2+}-activated channels could contribute to whole cell currents, we buffered intracellular Ca^{2+} with 10 mM EGTA to eliminate contribution of these endogenous channels. However, while the contribution of endogenous channels is suppressed in zero intracellular Ca^{2+}, the activity of TRPP2 is also suppressed by 80-90%[28]. As expected, in zero intracellular Ca^{2+}, WNT9B-induced PKD1/TRPP2-dependent currents were ~10-fold smaller than currents in 50 nM of intracellular Ca^{2+} and showed strong outward rectification, which is typical for members of the Polycystin family of ion channels[21, 29, 30] (Fig. 3b,h). The reversal potential was near −20 mV, consistent with the much higher K^+ permeability of TRPP2 compared to Na^+ or Ca^{2+} [31, 32]. Co-expression with $PKD1^{S99I}$ did not result in WNT9B-induced currents (Fig. 3c,h), as shown earlier (Fig. 2f). Co-transfection of PKD1 and the TRPP2 pathogenic mutant, $TRPP2^{D511V}$, suppressed the WNT9B response by ~75% compared to wild type TRPP2 (Fig. 3d,h). Cells co-transfected with PKD1 and pathogenic $TRPP2^{R872X}$ that does not interact with PKD1 failed to respond (Fig. 3e,h), indicating that the PKD1/TRPP2 interaction is required for the WNT9B response. Replacement of the pore-forming region of TRPP2 with the equivalent region of the K^+-permeable Kv1.3 ($TRPP2^{Kv1.3}$) suppressed inward currents but not outward currents carried by K^+ (Fig. 3f,h). The chimeric $TRPP2^{Kv1.3}$ channel was expressed in comparable levels to wild type TRPP2 and maintained its interactions with wild type TRPP2 or PKD1 (Supplementary Fig. 3c,d). These data suggested that TRPP2 directly contributed to the formation of WNT9B-induced currents and the interaction with PKD1 was required for the effect. PKD1L1 physically interacts with TRPP2[33, 34]. However, PKD1L1 did not interact with WNT9B (Fig. 1b). Consistently, it did not form a WNT9B-inducible channel complex in CHO-K1 cells (Fig. 3g,h). Overall, results from these experiments support the hypothesis that the PKD1/TRPP2 complex was activated by WNT9B, likely through a direct ligand-receptor interaction between WNT9B and PKD1. To test whether activation of the PKD1/TRPP2 channel involves activation of endogenous FZDs, we co-expressed ZNRF3 and tested for an effect on WNT9B-induced currents. ZNRF3 functions as an E3 ubiquitin ligase clearing FZDs from the cell surface[35]. ZNRF3 robustly suppressed WNT3A-induced activation of the WNT/β-canonical pathway which requires FZDs (Supplementary Fig. 3b), but had no effect on WNT9B-induced currents (Fig. 3h). These data suggested that PKD1/TRPP2 functioned independently of FZDs in CHO-K1 cells.

To further strengthen the evidence of FZD independent activation of TRPP2, we co-transfected PKD1 and TRPP2 into *Drosophila* S2 cells, which lack FZDs[36]. First, we showed that purified WNT9B bound to the cell surface of S2 cells transiently transfected with PKD1 and TRPP2 (Supplementary Fig. 4a-b). The pattern of cell surface-bound WNT9B was “spotty” suggesting that PKD1/TRPP2 channels are not uniformly distributed at the cell surface, as has been shown for *Drosophila* Fzd2[36]. Next, we showed that WNT9B (500 ng/ml) induced whole cell currents only in transfected cells (Supplementary Fig. 4c), providing additional evidence for the WNT-induced activation of PKD1/TRPP2 independently of FZDs.

TRPP2 mediates WNT-induced whole cell currents in MEFs

Wild type MEFs express PKD1[11] and TRPP2 (Fig. 6a and b and Supplementary Fig. 2d) and deletion of *Pkd2* is expected to cause an upregulation of the WNT/β-catenin pathway and constitutive activation of p38-MAPK[37]. Consistently, phospho-β-catenin levels were slightly decreased, whereas phospho-p38MAPK were slightly increased in *Pkd2*-null MEFs (Supplementary Fig. 5b,c). WNT3A induced activation of the canonical WNT/β-catenin pathway in *Pkd2* mutant cells and this increase was 2-3-fold higher compared to wild type cells (Supplementary Fig. 5g). Overexpression of ZNRF3 suppressed this effect (Supplementary Fig. 5h). Expression levels of *Fzd1/2/6/7/8,* and *Ryk* mRNAs or LRP6 and ROR2 proteins (LRP5 and ROR1 are not expressed in MEFs) were not different between wild type and *Pkd2*-null MEFs (Supplementary Fig. 5a,e,f). Expression level of DVL1 or DVL2 was similar between $Pkd2^{+/+}$ and $Pkd2^{-/-}$ cells, but slightly reduced in $Pkd1^{-/-}$ cells (Supplementary Fig. 5d). In sum, *Pkd2*-null cells showed higher activation of the canonical WNT/β-catenin pathway compared to wild type cells and no obvious differences in the expression levels of FZDs, ROR2, LRP6, and RYK receptors.

When intracellular Ca^{2+} was clamped at 50 nM, WNT9B induced large currents in wild type (Fig. 4a, black filled squares, c, red filled squares), but not *Pkd2*-null cells (Fig. 4a and c, blue open circles). WNT9B-induced currents showed a reversal potential at 0 mV and were reversibly blocked by La^{3+}, as was seen in CHO-K1 cells transfected with PKD1 and TRPP2 (Fig. 2e,h). In zero intracellular Ca^{2+}, WNT9B-induced whole cell currents showed outward rectification and a reversal potential close to −20 mV (Fig. 4d-f), as was seen in CHO-K1 cells transfected with PKD1 and TRPP2 under the same conditions (Fig. 3b). WNT9B did not induce a significant current in $Pkd2^{-/-}$ cells (Fig. 4d and f, blue open circles). Therefore, these experiments demonstrated that WNT9B was able to induce a similar current in native MEFs or CHO-K1 cells transfected only with PKD1/TRPP2, but not in *Pkd2*-null MEFs. The differential effect of WNT9B in wild type and *Pkd2*-null cells was specific, since both cell types responded similarly to extracellular ATP (Supplementary Fig. 6a-f). Adding-back wild type TRPP2 in mutant cells restored WNT9B-induced currents (Fig. 4g-i), whereas adding-back $TRPP2^{Kv1.3}$ restored only outward currents, but not inward currents (Fig. 4j-l), indicating that TRPP2 was directly involved in WNT9B-induced currents. Overexpression of ZNRF3 did not have an effect on WNT9B-induced currents (Fig. 4m-o) indicating that WNT9B-induced TRPP2-mediated currents were independent of FZDs and/or LRP6, as shown in CHO-K1 and *Drosophila* S2 cells.

Binding experiments showed that WNT3A was able to interact with the LRR-WSC domain of PKD1 (Supplementary Fig. 1). However, canonical WNT3A was not expected to induce Ca^{2+} signaling. At zero intracellular Ca^{2+}, WNT3A induced whole cell currents in wild type cells (Fig. 5a-c), but with a noticeable delay (by about a min) compared to WNT9B-induced currents (Fig. 4a,g). Expression of ZNRF3 did not have significant effects on current amplitude, whereas WNT3A failed to induce whole cell currents in *Pkd2*-null cells (Fig. 5g-i).

PKD1 interacts with DVL1 and DVL2, but DVLs do not affect WNT9B-induced PKD1/TRPP2-mediated currents

Next, we tested whether PKD1 could physically interact DVL1 and DVL2 (DVL3 is not present in these cells determined by RT-PCR). We found that DVL1 and DVL2 co-immunoprecipitated with PKD1 in wild type or *Pkd2*-null MEFs (Fig. 6a and b). Deletion analysis showed that DVL2 interacted with PKD1 and the interaction was abrogated by the E499G mutation in DVL2[38]. This mutation is located within the Dishevelled, Egl-10 and Plecstrin (DEP) domain (Fig. 6c), known to mediate the effects of DVL2 on PCP[39, 40]. It also impairs phosphorylation of DVL2[38]. Nevertheless, depletion of DVL2 or both DVL1 and DVL2 using RNAi (Fig. 6e) did not show a significant effect on WNT9B-induced whole cell currents (Fig. 6d), suggesting that although DVL1/2 physically interact with PKD1, they are not required for the formation of a functional PKD1/TRPP2 channel complex.

WNT9B-induced cell migration is dependent on TRPP2

WNT5A was shown to promote directional cell migration in a variety of cell types through a process involving both localized Ca^{2+} release transients originating from the cortical endoplasmic reticulum and Ca^{2+} influx[7]. Both types of Ca^{2+} signaling were required for directional cell migration through the formation of the WNT5A-mediated receptor-actin-myosin polarity structure in the trailing edge of a migrating cell[7]. Thus, we tested whether WNT9B could induce Ca^{2+} release. WNT9B did not induce Ca^{2+} release in wild type or *Pkd2*-null MEFs, in contrast to ATP which elicited a similar response (Supplementary Fig. 6g,h). Next, we tested whether WNT9B could promote directional cell migration in wild type and *Pkd2*-null MEFs, through TRPP2 and an increase in intracellular Ca^{2+} concentration. Wild type or *Pkd2*-null cells were stimulated with WNT9B for up to 2 h and the number of cells with a typical migratory phenotype (Fig. 7a) was determined in both cultures by double staining for F-actin and Myosin IIB. WNT9B failed to induce this migratory phenotype in *Pkd2*-null cells, whereas it had a strong effect on wild type cells (Fig. 7a,b). To test whether WNT9B-induced cell polarization was dependent on intracellular Ca^{2+}, $Pkd2^{+/+}$ MEFs were pretreated with DMSO or 10 μM BAPTA/AM for 45 min before adding WNT9B. BAPTA/AM blocked WNT9B-induced cell polarization (Fig. 7c) to a degree similar to *Pkd2*-null cells (Fig. 7b). To test whether *Pkd2*-null MEFs failed to polarize because of TRPP2, we added-back wild type TRPP2 or $TRPP2^{Kv1.3}$. Wild type, but not $TRPP2^{Kv1.3}$ rescued cell polarization in $Pkd2^{-/-}$ MEFs (Fig. 7d,e). Consistently, *Pkd2*-null cells failed to migrate towards a WNT9B gradient using a chemokinetic assay (Fig. 7f,g). In contrast to WNT9B, $Pkd2^{-/-}$ fibroblasts migrated normally in response to PDGF-BB (25 ng/ml) (Fig. 7h), a strong chemokinetic factor acting through Ca^{2+} flickers[41], store-, and/or receptor-activated Ca^{2+} channels[42], indicating that WNT9B-activated PKD1/TRPP2 mediated currents were distinct from the channels activated by PDGF-BB. Overall, these experiments showed that cells lacking TRPP2 exhibited reduced directional migration, suggesting that one of the functions of WNT9B-induced activated TRPP2 in cell culture is to establish polarization during directional cell migration.

PKD1 cooperates with DVL2 to maintain normal kidney tubulogenesis in *Xenopus* embryos

Next, we utilized *Xenopus* as a model organism[43, 44] to test whether PKD1 could function within the WNT pathway. We chose DVL2 to experimentally downregulate WNT signaling, because DVL2 is the major isoform expressed in the *Xenopus* pronephric kidney[45]. Knockdown of PKD1 using two independent splicing morpholinos (sMOs), one described in Xu et al[46] (*Pkd1-sMO1*) and another one (*Pkd1-sMO2*) described here (Supplementary Fig. 7), resulted in edema and dysplastic (dilated and shortened) pronephric tubules (Fig. 8i,l). Knockdown of DVL2 resulted in a cystic kidney phenotype grossly similar to PKD1 knockdown (Fig. 8i,l). Importantly, this phenotype could be reversed by co-injection of human *DVL2* mRNA, but not *DVL2-E499G* mRNA, which does not interact with PKD1 (Fig. 8m). Next, we combined a suboptimal dose of the *Pkd1-sMO1*, which by itself did not cause any cystic phenotype, with decreasing amounts of *Dvl2-MO* (Fig. 8a-i,l). The combined knockdown resulted in a synergistic effect compared to the individual MOs, suggesting a functional interaction between PKD1 and DVL2. Finally, injection of an MO targeting WNT9A (*Wnt9A-MO*), one of the WNT ligands specifically expressed in the pronephric kidney[43], on its own did not cause edema formation or dysplastic kidneys (Fig. 8j). However, combining *Wnt9-MO* with a suboptimal dose of *Pkd1-sMO1* demonstrated synergism (Fig. 8j-l) similar to the one observed for *Dvl2-MO* and *Pkd1-sMO1*. Together these data support the hypothesis that WNT9A, PKD1, and DVL2 function in the same pathway in pronephric development.

Discussion

Our data provide evidence that the PKD1/TRPP2 channel complex can function as a ligand-activated channel. Our data support the possibility of a direct ligand/receptor interaction for several reasons. First, the PKD1/WNT interaction does not require cell surface receptors, as it can occur in the extracellular space *in trans* and also, using purified proteins. Second, PKD1 is unlikely to function as a FZD or RYK co-receptor or downstream of these receptors, because neither WNT9B nor PKD1/TRPP2 induced or mediated Ca^{2+} release from the ER, an effect associated with FZD or RYK receptor activation[4, 6, 8]. Third, clearing FZDs and LRP6 from the cell surface did not suppress WNT9B-or WNT3A-induced currents and heterologous expression of PKD1 and TRPP2 in *Drosophila* S2 cells, which lack endogenous FZD receptors, supported WNT9B-induced currents. Therefore, PKD1 is likely to function as a (co)receptor for WNT ligands to induce Ca^{2+} influx, independently of FZD receptors. The fact that WNT3A, a typical canonical WNT activated TRPP2, a Ca^{2+} permeable channel, suggests that WNT ligands could induce Ca^{2+} influx regardless of their ability to signal through β-catenin as long as they can bind to PKD1 and PKD1/TRPP2 is present in the target cell. This may represent a general property of WNTs and implies a broader effect of WNTs on Ca^{2+} signaling than previously thought. It may also help explain the strong influence of cell context on WNT signaling.

We show that TRPP2 plays an important role in directional cell migration of MEFs in response to WNT9B. This is consistent with recent studies showing an essential role of PKD1 and TRPP2 in directional cell migration in embryonic kidney and endothelial cells

during lymphatic development[11, 47, 48]. Despite caveats, directed cell migration in cell culture has been used as a reliable surrogate assay for convergent extension during embryonic development[11]. Defective convergent extension was proposed to underlie cystogenesis in embryonic *Pkd1* and *Wnt9b* mutant kidneys[10, 11]. Although our data do not contradict this idea, we do not believe that defective convergent extension is the sole cause of cystogenesis in ADPKD, as deletion of core components of PCP, such as Vangl2, show very mild cystic dilatation[49]. We rather propose that defective WNT-induced PKD1/TRPP2-mediated Ca^{2+} signaling can adversely affect multiple processes, including convergent extension. Such a combinatorial effect can contribute to cyst initiation/formation.

Experiments in *Xenopus* embryos suggest that *xPkd1* genetically interacts with *xDvl2* in pronephric development. Overexpression of a dexamethasone-inducible, PCP-specific dominant negative form of *xDvl2* in *Xenopus* embryos produces dilated and shortened tubules[50], the same phenotype as the one modified by the combinatorial effects of *xPkd1* and *xDvl2*. We also show that PKD1 physically interacts with DVL2 and a point mutation in the DEP domain of DVL2 renders it unable to interact with PKD1. However, DVLs are dispensable for WNT9B-induced channel activity. These data suggest that DVL proteins can function as downstream effectors of PKD1/TRPP2 in the embryonic kidney. DVLs have been shown to function downstream of WNT/Ca^{2+} signaling by an unknown mechanism[8, 51]. One possibility is that the physical interaction between PKD1 and DVLs may function to keep the two proteins in close proximity so that incoming Ca^{2+} could directly impinge on DVLs or immediate downstream effectors.

We show that several WNTs can bind to PKD1. These data suggest that PKD1/TRPP2 can mediate effects of other WNTs not only in the kidney but in other tissues where WNT/Ca^{2+} activity is present. This is supported by the ubiquitous expression of PKD1 and TRPP2 and the wider phenotypic spectrum caused by the homozygous deletions of *Pkd1* or *Pkd2* genes compared to the phenotypic spectrum of patients with autosomal dominant PKD. We speculate that renal (cystogenesis), cardiovascular (heterotaxy, defective septation, lymphatic development)[47, 48, 52-54], hearing (inner ear architecture)[55], hydrocephalus [56, 57] and skeletal defects (neural crest cell migration, spina bifida, osteoblast differentiation)[58-60] in *Pkd1*- or *Pkd2*-null mice may represent *bona fide* defects of the WNT/Ca^{2+} signaling pathway.

METHODS

Animals

Studies using *Xenopus* embryos were approved by the Institutional Animal Care and Use Committee and adhered to the National Institutes of Health Guide for the Care and Use of Laboratory Animals.

Cell lines

HEK293, HEK293T, and CHO-K1 cell lines were obtained as authenticated stocks from ATCC. Wild type, *Pkd1*$^{-/-}$, and *Pkd2*$^{-/-}$ cells were obtained from The Baltimore PKD Center (http://www.baltimorepkdcenter.org/). *Drosophila* Schneider S2 cells were purchased from Invitrogen. The HEK293 cell line has been misidentified according to ICLAC, but it

was only used here to overexpress PKD1 fragments as Fc fusions and myc-tagged WNT5A due to its high transfectability. All cells lines were tested negative for mycoplasma using PCR and DAPI staining. HEK293 or HEK293T cells were maintained in DMEM supplemented with 10% FBS. CHO-K1 were grown in Ham's F-12/DMEM with 10% FBS. *Pkd1*$^{-/-}$ *and Pkd2*$^{-/-}$ mouse embryonic fibroblasts (MEFs) and wild type littermate type control cells were cultured in DMEM supplemented with 10% heat inactivated FBS, 1% non-essential amino acids, and 1% penicillin-streptomycin.

Reagents

Purified WNT9B and WNT3A were purchased in a carrier-free formulation from R&D.

Transfections

CHO-K1 cells were transfected by Lipofectamine2000 (Invitrogen) according to manufacturer's recommendations. HEK293T cells were transfected with the calcium phosphate precipitation method. MEFs were transfected by Nucleofection (Lonza), according to manufacturer's recommendations. In a typical transfection reaction, 2×10^6 wild type MEFs were transfected with 0.2 μg CD8α and 20 pm (20 μM) of siRNAs or 1.8 μg of plasmid DNA (ie, wild type TRPP2) using Nucleofector (Program T-20, MEF Kit 2, Lonza).

Immunoprecipitations

In experiments where immunoprecipitations were done in lysates, cells were lysed in 1% Triton X-100, 150 mM NaCl, 10 mM Tris-HCl at pH 7.5, 1 mM EDTA, 1 mM EGTA, 0.5% NP-40, and 10% sucrose with protease inhibitor cocktail (Roche Applied Science) at 4°C for 30 min and lysates were collected by centrifugation (18,000 × g, 20 min). In immunoprecipitations using cultured media, media were collected and filtered (Millipore). Lysates (500 μl) or filtered media (1 ml) were incubated at 4°C for overnight with indicated antibodies listed in **Suppl. Table 1** coupled to Sepharose beads. Beads were pelleted by centrifugation, and pellets were washed in lysis buffer three times for 20 min with rotation at 4°C. Immunoprecipitated proteins immunoblotted with indicated antibodies as listed in **Suppl. Table 1**.

siRNAs used in this study are listed in **Suppl. Table 2**.

Plasmids

Expression plasmids carrying human WNT9B and Flag-PKD1L1 cDNAs were purchased from Origene. WNT3A, WNT4, WNT5A, and mouse TRPP2 plasmids were obtained from Open Biosystems (Thermo). Mouse FZD8-CRD-Fc construct was obtained from Addgene. Flag-tagged mouse PKD1 and human HA-tagged PKD1 were provided by Drs. Yang (Columbia) and Qian (University of Maryland), respectively. ZNRF3 was obtained from Dr. Cong (Novartis). Human TRPP2^{D511V} and TRPP2^{R872X,} and mutant forms of mouse LRR-Fc and human full-length PKD1 were generated using the QuikChange mutagenesis kit according to the manufacturer's instructions (Stratagene). The LRR-WSC domain of mouse PKD1 (amino acid residues 24-255), LDL-A domain of mouse PKD1 (amino acid residues 397-671), and first PKD domain of human PKD1 (amino acid residues 282-353) were cloned into the pAP3 vector [61] that contained the signal sequence of K-cadherin fused to the

alkaline phosphatase cDNA. The thermostable placental alkaline phosphatase cDNA was replaced with the CH2-CH3 region of human IgG (Fc) to generate LRR-WSC-Fc, LDL-A-Fc and hPKD1(d1)-Fc constructs, respectively. TRPP2$^{Kv1.3}$ was made by replacing the extracellular loop connecting transmembrane segments 5 and 6, from amino acid residue 617 to 665 of human TRPP2 (NP_000288) with the equivalent loop of mouse Kv1.3 (NP_032444) from amino acid residue 366 to 448. 3xFlag-tagged DVL2, DVL2-dPY, DVL2-dDIX, and DVL2-E499G were gifts from Jeff Wrana (Addgene plasmid #s: 24802, 24808, 24805, and 24803, respectively) and TRPP2-Myc (or M-PKD2) was a gift from Gregory Germino (Addgene plasmid #:21370).

Protein-protein interactions using purified proteins

The LRR-WSC domain of PKD1 fused to human IgG (LRR-WSC-Fc) was stably transfected into HEK293 cells. Five 10-cm dishes containing confluent cultures of HEK293/LRR-WSC-Fc cells were conditioned for 4 days in Optimem. LRR-WSC-Fc was captured using protein G and beads were washed ten times (20 min each) with immunoprecipitation solution where the NaCl concentration was adjusted to 1M to minimize interaction with proteins present in the extracellular solution. After the final wash, beads were reconstituted in normal immunoprecipitation solution (150 mM NaCl) and incubated with 500 ng of purified WNT9B in 0.05% BSA in 1 ml total volume overnight at 4°C. Unbound WNT9B was removed by four 20-min washes at 4°C. Bound WNT9B was detected by immunoblotting using goat α-WNT9B. To determine direct binding of WNT9B to TRPP2, six 10-cm dishes of HEK293T cells were transiently transfected with a Myc-tagged form of human TRPP2. Myc-tagged TRPP2 was pulled down using α-Myc and washed 10 times (20 min each) in normal immunoprecipitation solution (150 mM NaCl). Beads containing Myc-TRPP2 were incubated with 500 ng of purified WNT9B in 0.05% BSA in 1 ml immunoprecipitation solution overnight at 4°C. Beads were washed four times (20 min each) with immunoprecipitation solution to remove unbound WNT9B. Bound WNT9B was detected by immunoblotting using goat α-WNT9B. Protein quantification was done by the LI-COR Odyssey® Fc imaging system.

Ratiometric single cell Ca^{2+} imaging

CHO-K1 cells were plated onto glass coverslips and placed in 35-mm dishes where they were transfected with full length mouse PKD1, TRPP2, and yellow fluorescent protein (YFP) cDNAs using Lipofectamin2000 (Invitrogen). Twenty four hours after transfection cells were loaded with 2 μM Fura-2/AM in extracellular solution (ECS) containing 140 mM NaCl, 5 mM KCl, 1 mM $MgCl_2$, 1.8 mM $CaCl_2$, 10 mM glucose, and 15 mM Hepes, pH 7.4, ($[Ca^{2+}]_o$: 1.8mM) in the presence of 0.05% Pluronic F-127 for 45 min at room temperature. Cells were washed twice in ECS and incubated for 15 min in 37° C before intracellular imaging. Coverslips were mounted onto the stage of an Axiovert200 inverted microscope and cells were perfused with ECS or 500 ng/ml WNT9B in ECS for 30 min. Ionomycin (2 μM) was added towards the end of the experiment (time point 35 min) to induce maximum Ca^{2+} entry. To determine the effect of WNT9B on transfected cells in nominally Ca^{2+}-free extracellular solution, cells were perfused with ECS for 5 min and then ECS was switched to a Ca^{2+}-free extracellular solution (same as ECS but without $CaCl_2$ plus 10μM EGTA) with or without WNT9B (500 ng/ml) for 30 min. Ca^{2+} (1.8 mM) was

added back at time point 35 min. Singly transfected cells were identified using a YFP filter set and imaged using a Fura-2 filter set with a CCD camera (CoolSnap HQ, Photomertrics) driven by the Metafluor software (Universal Imaging). Fluorescence ratios of 340/380 were taken every 1 s using 200 ms exposure time. Changes in intracellular Ca^{2+} concentration ($\Delta[Ca^{2+}]_i$) was expressed as 340/380 ratio. Traces represent average fluorescence ratio 340/380 over time from 50-65 cells pooled from 3-5 independent experiments.

Pkd2$^{+/+}$ and *Pkd2*$^{-/-}$ MEFs were plated onto glass coverslips. Twenty four hours after seeding, cells were loaded with 2 μM Fura-2/AM in Ca^{2+}-free extracellular solution (same as ECS but without $CaCl_2$ plus 10μM EGTA) in the presence of 0.05% Pluronic F-127 for 45 min at room temperature. Cells were washed twice in ECS-Ca^{2+} free and incubated for 15 min in 37° C before intracellular imaging. Coverslips were mounted onto the stage of an Axiovert200 inverted microscope and cells were treated with 500 ng/ml WNT9B followed by 100 μm ATP at the end of experiment. Cells (47 for *Pkd2*$^{+/+}$, 37 for *Pkd2*$^{-/-}$) were imaged using a Fura-2 filter set with a scientific CMOS camera (Pco.Edge Scientific) controlled by EasyRatioPro software (PTI). Fluorescence ratios of 340/380 were taken every 1 s using 200 ms exposure time. Changes in intracellular Ca^{2+} concentration ($\Delta[Ca^{2+}]_i$) was expressed as 340/380 ratio. Traces represent average fluorescence ratio 340/380 over time from 37-47 cells pooled from 3 independent experiments.

Electrophysiology

Immediately before each experiment, a coverslip bearing CHO-K1 or MEFs was removed from the culture plate and placed onto a recording chamber, which was mounted on the stage of a Nikon Diaphot inverted microscope. The extracellular solution was normal Tyrode solution containing (in mM): 135 NaCl, 5.4 KCl, 0.33 NaH_2PO_4, 1 $MgCl_2$, 1.8 $CaCl_2$, 5 HEPES, 5.5 glucose (pH 7.4). Pipettes were made from capillary glass (plain; Fisher Scientific, Pittsburgh, PA, USA) with a micropipette puller and polisher (PP-830 and MF-830, respectively; Narishige, Tokyo, Japan). They were back-filled with internal solution composed of (in mM): 100 K-aspartate, 30 KCl, 0.3 Mg-ATP, 10 HEPES, 10 EGTA, and 0.03 GTP (pH 7.2). In experiments where intracellular Ca^{2+} was clamped to 50 nM, 4 mM $CaCl_2$ was added to the internal solution. The pipette resistance varied from 3–5 MΩ when filled with the internal solution. Offset potential was corrected just before a gigaohm seal formation. Series resistance and capacitance transients were compensated when CHO-K1 cells were used with a Warner PC-505B amplifier (Warner Instrument Corp., Hamden, CT, USA) and pClamp 10.0 software (Axon Instrument, Foster City, CA, USA). Cell capacitance was not compensated in MEFs due to their large size (>100pF). Currents were digitized with a Digidata 1440A converter (Molecular Devices), filtered through an internal four-pole Bessel filter at 1 kHz, and sampled at 2 kHz. Inward and outward whole-cell currents were obtained by employing a step-pulse protocol from −100 to +100mV every 5 s for 200 ms duration from a holding potential of −60mV. I-V curves were taken before and 5 min after the addition of WNT9B or WNT3A in the bath solution and derived from a step protocol ranging from −100 to +100 mV with 20 mV increments for 200 ms duration from a holding potential of −60mV. Steady-state currents towards the end of the pulse (between 50 and 100 ms) were used in I-V curves. Cells with a similar diameter displaying similar in magnitude stable baseline currents among various groups were selected for

recordings and used for further analysis. WNT9B or WNT3A stock solution (100 ng/μl) was dissolved in Tyrode solution and added directly to the recording chamber. Current traces were analyzed off-line with pClamp 10.0.

Indirect immunofluorescence

MEFs were seeded on poly L-lysine coated glass coverslips (8×10^4 cells/6-well plate/coverslip) for 24 h, washed and starved for 18 h. WNT9B (500 ng/ml) was added at time 0 and cells were incubated at 37°C for 30, 60, and 120 min. Cells were fixed in 10% formalin solution (Sigma-Aldrich) at room temperature (RT), permeabilized with 0.2 % Triton X-100 in PBS, blocked in 5% BSA, 0.1% Tween/Tris-buffered saline and incubated with rabbit α-Myosin II B (Sigma-Aldrich, 1:200) in blocking buffer at RT for 1 hr. Cells were washed with PBS and incubated with donkey anti-rabbit Alexa 568 secondary antibody (Molecular Probes, 1:2000) and phalloidin coupled to Alexa 488 (Molecular Probes, 1:40) for 1 h at RT. DNA was stained with 5 μg/ml DAPI for 10 min. Coverslips were mounted with ProLong (Molecular Probes), and cells were imaged using an Olympus IX81 inverted confocal microscope. Images were analyzed by the Olympus Fluoview software.

Rescue experiments

Two million *Pkd2*$^{-/-}$ cells were transfected with GFP+pCDNA3 (mock), GFP+wild type TRPP2 (TRPP2^{WT}), or GFP+TRPP2$^{Kv1.3}$ expression plasmids using nucleofection. Transfection efficiency was 20-30% as determined by GFP. Eighteen hours following transfection, cells were seeded on poly L-lysine coated coverslips, serum-starved for 18 h, and stimulated with purified WNT9B (500 ng/ml) or PBS for 1 h. Cells were fixed and double-stained with phalloidin-Texas Red and α-Myosin II B as described above. Twenty six to thirty nine confocal images containing 4-12 GFP-positive cells were randomly collected from each group and the number of GFP-positive migrating cells per field was recorded. The total number of cells scored per group was 366 (pcDNA3), 352 (TRPP2^{WT}) and 390 (TRPP2$^{Kv1.3}$). Three independent transfections (experiments) using identical conditions (except for cell passage number) were done with similar results.

Chemokinetic assay

After serum starvation for 18 h, *Pkd2*$^{+/+}$ or *Pkd2*$^{-/-}$ MEFs (5×10^4/insert) were seeded in inserts (8 μm in pore size, BD Biosciences), which were placed in 24-well dish containing 500 μl of media supplemented with 0.1% FBS and PBS, WNT9B (1 μg/ml) or PDGF-BB (25 ng/ml). Cells were allowed to migrate through inserts for 6 h at 37°C. Cells in the lower side of inserts facing the bottom of the well were fixed with methanol, stained with hematoxylin and eosin, and counted. Quantification of migrating *Pkd2*$^{+/+}$ or *Pkd2*$^{-/-}$ cells was obtained from 3 independent experiments done in sextuplicates (WNT9B) or quadruplicates (PDGF-BB).

Functional expression of PKD1 and TRPP2 in *Drosophila* S2 cells

-Molecular cloning and expression—The *Bgl2-Age1* fragment encompassing ~13 kb of human PKD1 cDNA was moved from HA-PKD1 (HBF307N-hPKD1) to the *Drosophila* pMT/V5-HisA vector (Invitrogen). The remaining 5’ part of the cDNA was

amplified by PCR incorporating the *Drosophila* optimal translational initiation start site (CAAA) immediately upstream of the first methionine and was cloned into pMT/V5-HisA upstream of the *Bgl2-Age1* fragment of human PKD1 using *EcoR1* (5') and *Bgl2* (3'). The *EcoR1-Bgl2* fragment of PKD1 in pMT/V5-HisA was verified by complete sequencing. Mouse TRPP2 bearing the CAAA sequence upstream of its first methionine was cloned into the pMT/V5-HisA vector as *EcoR1-Xho1* fragment. The human CD8α cDNA excluding the nucleotide sequence corresponding to the signal peptide was cloned into the pMT/Bip/V5-HisA vector as a *Kpn1-EcoR1* fragment. CD8α or PKD1+TRPP2 in pMT/BIP or pMT vectors were transiently transfected into *Drosophila* S2 cells using Nucleofection (Program G-30, transfection kit V, Amaxa). Transfection was done in 12-well plates containing 2×10^6 (for functional expression) or 10^7 cells (for biochemical expression) using 2 μg of total DNA (1.5 μg PKD1, 0.3 μg TRPP2, and 0.2 μg CD8α). Transfection efficiency using pMT/GFP was routinely at 80-90%. Cells were treated with 700 μM $CuSO_4$ 24 h following transfection and for 48 h to induce the expression of CD8α, PKD1, and TRPP2.

-Electrophysiology—Twenty four hours following induction by CuSO4 (700 μM), cells were seeded onto poly-L-lysine coated coverslips and processed for electrophysiology after another 24 h. Whole cell currents were obtained as described above for MEFs and CHO-KI cells with the following exceptions: Pipette resistance was 6 MΩ when back-filled with intracellular solution where the Ca^{2+} concentration was adjusted to 100 nM (physiological). Typical capacitance was 9-11 pF. Extracellular solution was Tyrode solution. Cell capacitance was not compensated.

-WNT9B cell surface binding—Cells were seeded onto poly-L-lysine-coated glass disks the day before the experiment. At the day of the experiment, cells were washed twice with PBS and incubated with 1 μg/ml purified WNT9B in 0.5% BSA at 4°C for 3 h. Cells were washed three times (10 min each wash) with cold PBS and fixed in 2% paraformaldehyde in PBS for 15 min at room temperature. Cells were washed three times with cold PBS and incubated overnight with 1:500 dilution (or 0.4 μg/ml) of goat α-WNT9B in 5% donkey serum in PBS. Next day, cells were washed there times in cold PBS and incubated for 1 h with donkey α-goat conjugated to Alexa-488. After three final washes with cold PBS, coverslips were mounted with ProLong (Molecular Probes), and cells were imaged using an Olympus IX81 inverted confocal microscope (60x). Images were analyzed by the Olympus Fluoview software.

TOP/FOP Flash reporter assays—One million of MEFs or CHO-K1 cells were transfected with a Super TOP-Flash or FOP-Flash plasmid and Renilla luciferase pRL-TK vector together with pcDNA3 or ZNRF3 expression vector, using the Ingenio Electroporation Kit (Mirus-Bio) and the Nucleofector IIb Device (Lonza). Renilla luciferase was used as the internal control reporter to normalize transfection efficiency. All transfections were performed with 0.5 μg of Super TOP-Flash or FOP-Flash, 0.05 μg of pRL-TK, and 2 μg of pCDNA3 or ZNRF3. After 18 h following transfection, cells were split into 18 wells of a 24 well plate. After 24 hr, cells were treated with PBS, WNT3A (500 ng/ml), WNT9B (1 μg/ml), or a mixture of WNT3A and WNT9B for another 24 hr and lysed in a reporter lysis buffer (Promega, Madison, WI, USA). Luciferase assay was performed using

the Dual Luciferase Assay System kit according to the manufacturer's protocols (Promega, Madison, WI, USA). Relative luciferase activity was reported as fold induction after normalization for transfection efficiency. Three independent experiments were performed in sextuplicates.

RNA-isolation and Quantitative RT PCR—Total RNA from *Pkd2*$^{+/+}$ and *Pkd2*$^{-/-}$ MEFs was extracted using Trizol reagent (Invitrogen, Carlsbad, CA) according to the manufacturer's instructions. 5 μg of total RNA was used for cDNA synthesis with 1:1 mixture of 50 ng/μl random hexamers (Invitrogen) and 0.5 μg/μl Oligo dT (Invitrogen). Quantitative real-time PCR were performed on the resultant cDNA using the PerfeCTa CYBR Green SuperMix for iQ (Quanta BioSciences, Gaithersburg, MD) following manufacturer's instructions. Primer sequence information is presented in **Suppl. Table 2**. Real-time PCR was carried out using a Bio-Rad iCycler Thermal Cycler (Bio-Rad, Hercules, CA). Reactions were run in triplicate in three independent experiments. The mRNA levels of each target protein were normalized relative to housekeeping gene GAPDH mRNA levels in each sample.

Xenopus* Embryo Manipulations—Xenopus* embryos obtained by *in vitro* fertilization were maintained in 0.1x modified Barth medium [62] and staged according to Nieuwkoop and Faber [63]. The sequences of the antisense morpholino oligomers (GeneTools, LLC) used in this study are listed in **Suppl. Table 2**. The efficacy of *Dvl2-MO* and *Pkd1-sMO1* was demonstrated previously[64, 65]. The efficacy of *Pkd1-sMO2* was verified by RT-PCR of RNA extracted from stage 35 embryos (Supplementary Fig. 7e) using primers spanning exons 17/18 of the predicted *Xenopus laevis Polycystin1* (Xenbase Gene #483413, 5'-TGT CCT TGA AGT GCG TGT CA-3' and 5'-CCC GTA GAT GTG GTG CTT GA-3').In the case of *Wnt9A-MO*, it was verified using a Wnt9A-GFP fusion construct injected into *Xenopus* embryos in the presence or absence of the *Wnt9A-MO*. For morphological scoring of edema formation embryos were injected at the 2- to 4-cell stage with the indicated amounts of MO and cultured until sibling embryos reaches stage 43. For whole the imaging of the individual pronephric kidneys embryos were injected unilaterally at the 2-cell stage embryo with the indicated amounts of MOs, cultured until stage 40 and fixed in Dent's fixative (4:1 Methanol:DMSO). Whole mount immunofluorescence was performed by incubating the embryos sequentially with the 3G8 and 4A6 antibodies[66] and developing them using AlexaFluor-448 and AlexaFluor-555-labeled α-mouse secondary antibodies (Life Technologies). Embryos were analyzed individually by confocal microscopy comparing the injected to the contralateral control side. Pronephric kidneys with dilated and shortened nephron segments were classified as dysplastic. In individual cases 3-dimensional (3D) reconstruction of the kidneys was used to verify differences in tubule diameter. Analysis was performed in a blinded fashion to avoid bias.

Rescue experiments for the *Dvl2-MO* were performed by injecting 0.5 μg synthetic mRNA encoding wild type human *DVL2* or mutant *DVL2-E499G* into a single blastomere at the 2-cell stage followed by injection of 3.2 pMol *Dvl2-MO* into all four blastomeres at the 4-cell stage. Embryos were cultured until stage 40 and processed for whole kidney imaging as

outlined above. Scoring was based on comparing the kidneys of the *Dvl2-MO*-injected side to the one of the *Dvl2-MO*/mRNA-injected side

Cell surface biotinylation—Wild type, *Pkd1*$^{-/-}$ MEFs, or HEK293T cells co-transfected with TRPP2 and wild type PKD1 (PKD1^{WT}) or PKD1^{S99I} were washed 3 times in PBS (pH 8.0), scraped, and re-suspended in 1 ml PBS (pH 8.0). Cell surface proteins were labelled with 1 mM EZ-Link NHS-PEG4-biotin (Thermo Scientific, 21329) for 30 min at room temperature. Biotinylation was terminated by 3 washes with PBS containing 100 mM Glycine, pH 3.0, and lysed in 1% Triton X-100, 150 mM NaCl, 10 mM Tris-HCl at pH 7.5, 1 mM EDTA, 1 mM EGTA, 0.5% NP-40, and 10% sucrose with protease inhibitor cocktail (Roche Applied Science) at 4°C for 30 min. Lysates were collected by centrifugation (18,000 × g, 20 min) and biotin-labelled surface proteins were captured on streptavidin–agarose beads at 4°C by an overnight incubation. Proteins bound to beads were collected by a brief (1 min) centrifugation, and pellets were washed 3 times with lysis buffer for 20 min at 4°C. Biotin-labeled surface proteins were eluted with SDS gel-loading buffer (50 mM Tris-HCl at pH 6.8, 100 mM DTT, 2% SDS, 0.1% bromophenol blue, and 10% glycerol) and analyzed by western blotting.

Endogenous co-immunoprecipitations—Five 10-cm dishes containing confluent cultures of wild type MEFs were pooled and lysed in 1 ml of non-denaturing lysis buffer containing 1% Triton X-100, 150 mM NaCl, 10 mM Tris-HCl at pH 7.5, 1 mM EDTA, 1 mM EGTA, 0.5% NP-40, and 10% sucrose with protease inhibitor cocktail (Roche Applied Science) at 4°C for 30 min. Lysates were cleared by centrifugation (18,000 × g, 20 min) and incubated with either mouse α-PKD1 (E4, 5 μg) or mouse IgG (Santa Cruz biotechnology) at 4°C overnight. Mouse antibodies were captured by Protein G coupled to agarose beads and immunocomplexes were immunoblotted with rabbit α-Dvl1 (1:200, Thermo Fisher, Rockford, IL, USA), rabbit α-Dvl2 (1:1000, Thermo Fisher) or mouse α-PKD1 (7e12, 1:5,000). Proteins were visualized with an enhanced chemiluminescence detection kit (ECL, Thermo).

Statistics and reproducibility

Student's *t* test was used for pairwise comparisons (ie, current amplitudes at defined membrane voltages before and after WNT9B or WNT3A in all I-V curves). One way ANOVA followed by Newman-Keuls *post hoc* test was used to analyze data for multiple comparisons. All results are presented as means (± S.E.M). N.S., indicates no significance; *, indicates $P<0.05$; **, indicates $P<0.01$; ***, indicates $P<0.001$. No statistical method was used to predetermine sample size. The experiments were not randomized. Evaluations of edema counts and dysplastic kidneys were performed in a blinded way, so that the person scoring embryos for edema or dilated and shortened tubules was not aware of the genotype of the animals. For electrophysiology experiments, n indicates the total number of cells per group that were successfully patched and summary data were derived from. One cell is considered to be one biologically replicate sample. Cells were pooled across independent experiments as indicated in the figure legends.

Supplementary Material

Refer to Web version on PubMed Central for supplementary material.

ACKNOWLEDGEMENTS

We would like to thank Drs. A. Pioszak, R. Janknecht, M. Ahmad, D. Sherry, and L. Rothblum for comments on the manuscript, Drs. J. Yang for mouse Flag-tagged PKD1, F. Qian for human HA-tagged PKD1 and E4 mouse monoclonal antibody against PKD1, F. Cong for ZNRF3 plasmid, E. Petsouki and V. Gerakopoulos in the Tsiokas lab for help with confocal imaging and immunoblotting in S2 cells. This work was supported by grant number 81270098 from NSFC (HN), DK080745 from NIH (OW), DK59599 from NIH (LT), Oklahoma Center for the Advancement of Science and Technology (LT), Oklahoma Center for Adult Stem Cell Research (LT), and the John S. Gammill Endowed Chair in Polycystic Kidney Disease (LT). These studies utilized reagents provided by the NIDDK sponsored Baltimore Polycystic Kidney Disease Research and Clinical Core Center, P30DK090868.

REFERENCES

1. MacDonald BT, Tamai K, He X. Wnt/beta-catenin signaling: components, mechanisms, and diseases. Dev Cell. 2009; 17:9–26. [PubMed: 19619488]
2. Angers S, Moon RT. Proximal events in Wnt signal transduction. Nat Rev Mol Cell Biol. 2009; 10:468–477. [PubMed: 19536106]
3. Logan CY, Nusse R. The Wnt signaling pathway in development and disease. Annu Rev Cell Dev Biol. 2004; 20:781–810. [PubMed: 15473860]
4. Kuhl M, Sheldahl LC, Park M, Miller JR, Moon RT. The Wnt/Ca2+ pathway: a new vertebrate Wnt signaling pathway takes shape. Trends Genet. 2000; 16:279–283. [PubMed: 10858654]
5. Slusarski DC, Corces VG, Moon RT. Interaction of Wnt and a Frizzled homologue triggers G-protein-linked phosphatidylinositol signalling. Nature. 1997; 390:410–413. [PubMed: 9389482]
6. Sheldahl LC, et al. Dishevelled activates Ca2+ flux, PKC, and CamKII in vertebrate embryos. J Cell Biol. 2003; 161:769–777. [PubMed: 12771126]
7. Witze ES, et al. Wnt5a directs polarized calcium gradients by recruiting cortical endoplasmic reticulum to the cell trailing edge. Dev Cell. 2013; 26:645–657. [PubMed: 24091015]
8. Lin S, Baye LM, Westfall TA, Slusarski DC. Wnt5b-Ryk pathway provides directional signals to regulate gastrulation movement. J Cell Biol. 2010; 190:263–278. [PubMed: 20660632]
9. Hutchins BI, Li L, Kalil K. Wnt/calcium signaling mediates axon growth and guidance in the developing corpus callosum. Developmental neurobiology. 2011; 71:269–283. [PubMed: 20936661]
10. Karner CM, et al. Wnt9b signaling regulates planar cell polarity and kidney tubule morphogenesis. Nat Genet. 2009; 41:793–799. [PubMed: 19543268]
11. Castelli M, et al. Polycystin-1 binds Par3/aPKC and controls convergent extension during renal tubular morphogenesis. Nature communications. 2013; 4:2658.
12. Piontek K, Menezes LF, Garcia-Gonzalez MA, Huso DL, Germino GG. A critical developmental switch defines the kinetics of kidney cyst formation after loss of Pkd1. Nat Med. 2007; 13:1490–1495. [PubMed: 17965720]
13. Hughes J, et al. The polycystic kidney disease 1 (PKD1) gene encodes a novel protein with multiple cell recognition domains. Nat Genet. 1995; 10:151–160. [PubMed: 7663510]
14. Consortium IPKD. Polycystic kidney disease: the complete structure of the PKD1 gene and its protein. The International Polycystic Kidney Disease Consortium. Cell. 1995; 81:289–298. [PubMed: 7736581]
15. Parnell SC, et al. The polycystic kidney disease-1 protein, polycystin-1, binds and activates heterotrimeric G-proteins in vitro [In Process Citation]. Biochem Biophys Res Commun. 1998; 251:625–631. [PubMed: 9792824]
16. Tsiokas L, Kim E, Arnould T, Sukhatme VP, Walz G. Homo- and heterodimeric interactions between the gene products of PKD1 and PKD2. Proc Natl Acad Sci U S A. 1997; 94:6965–6970. [PubMed: 9192675]

17. Qian F, et al. PKD1 interacts with PKD2 through a probable coiled-coil domain. Nat Genet. 1997; 16:179–183. [PubMed: 9171830]
18. Mochizuki T, et al. PKD2, a gene for polycystic kidney disease that encodes an integral membrane protein. Science. 1996; 272:1339–1342. [PubMed: 8650545]
19. Hanaoka K, et al. Co-assembly of polycystin-1 and -2 produces unique cation-permeable currents. Nature. 2000; 408:990–994. [PubMed: 11140688]
20. Bai CX, et al. Formation of a new receptor-operated channel by heteromeric assembly of TRPP2 and TRPC1 subunits. EMBO reports. 2008; 9:472–479. [PubMed: 18323855]
21. Bai CX, et al. Activation of TRPP2 through mDia1-dependent voltage gating. Embo J. 2008; 27:1345–1356. [PubMed: 18388856]
22. Kottgen M, et al. TRPP2 and TRPV4 form a polymodal sensory channel complex. J Cell Biol. 2008; 182:437–447. [PubMed: 18695040]
23. Zhang ZR, et al. TRPP2 and TRPV4 form an EGF-activated calcium permeable channel at the apical membrane of renal collecting duct cells. PloS one. 2013; 8:e73424. [PubMed: 23977387]
24. Bourhis E, et al. Reconstitution of a frizzled8.Wnt3a.LRP6 signaling complex reveals multiple Wnt and Dkk1 binding sites on LRP6. J Biol Chem. 2010; 285:9172–9179. [PubMed: 20093360]
25. Delmas P, et al. Gating of the polycystin ion channel signaling complex in neurons and kidney cells. FASEB J. 2004; 18:740–742. Epub 2004 Feb 2006. [PubMed: 14766803]
26. Giamarchi A, et al. A polycystin-2 (TRPP2) dimerization domain essential for the function of heteromeric polycystin complexes. Embo j. 2010; 29:1176–1191. [PubMed: 20168298]
27. Tan YC, et al. Novel method for genomic analysis of PKD1 and PKD2 mutations in autosomal dominant polycystic kidney disease. Human mutation. 2009; 30:264–273. [PubMed: 18837007]
28. Cantero Mdel R, Cantiello HF. Calcium transport and local pool regulate polycystin-2 (TRPP2) function in human syncytiotrophoblast. Biophys J. 2013; 105:365–375. [PubMed: 23870258]
29. Kim I, et al. Fibrocystin/polyductin modulates renal tubular formation by regulating polycystin-2 expression and function. J Am Soc Nephrol. 2008; 19:455–468. [PubMed: 18235088]
30. DeCaen PG, Delling M, Vien TN, Clapham DE. Direct recording and molecular identification of the calcium channel of primary cilia. Nature. 2013; 504:315–318. [PubMed: 24336289]
31. Luo Y, Vassilev PM, Li X, Kawanabe Y, Zhou J. Native polycystin 2 functions as a plasma membrane Ca2+-permeable cation channel in renal epithelia. Mol Cell Biol. 2003; 23:2600–2607. [PubMed: 12640140]
32. Ma R, et al. PKD2 functions as an epidermal growth factor-activated plasma membrane channel. Mol Cell Biol. 2005; 25:8285–8298. [PubMed: 16135816]
33. Kamura K, et al. Pkd1l1 complexes with Pkd2 on motile cilia and functions to establish the left-right axis. Development. 2011; 138:1121–1129. [PubMed: 21307098]
34. Field S, et al. Pkd1l1 establishes left-right asymmetry and physically interacts with Pkd2. Development. 2011; 138:1131–1142. [PubMed: 21307093]
35. Hao HX, et al. ZNRF3 promotes Wnt receptor turnover in an R-spondin-sensitive manner. Nature. 2012; 485:195–200. [PubMed: 22575959]
36. Bhanot P, et al. A new member of the frizzled family from Drosophila functions as a Wingless receptor. Nature. 1996; 382:225–230. [PubMed: 8717036]
37. Kim I, et al. Conditional mutation of Pkd2 causes cystogenesis and upregulates beta-catenin. J Am Soc Nephrol. 2009; 20:2556–2569. [PubMed: 19939939]
38. Narimatsu M, et al. Regulation of planar cell polarity by Smurf ubiquitin ligases. Cell. 2009; 137:295–307. [PubMed: 19379695]
39. Axelrod JD, Miller JR, Shulman JM, Moon RT, Perrimon N. Differential recruitment of Dishevelled provides signaling specificity in the planar cell polarity and Wingless signaling pathways. Genes Dev. 1998; 12:2610–2622. [PubMed: 9716412]
40. Boutros M, Paricio N, Strutt DI, Mlodzik M. Dishevelled activates JNK and discriminates between JNK pathways in planar polarity and wingless signaling. Cell. 1998; 94:109–118. [PubMed: 9674432]
41. Wei C, et al. Calcium flickers steer cell migration. Nature. 2009; 457:901–905. [PubMed: 19118385]

42. Bisaillon JM, et al. Essential role for STIM1/Orai1-mediated calcium influx in PDGF-induced smooth muscle migration. Am J Physiol Cell Physiol. 2010; 298:C993–1005. [PubMed: 20107038]
43. Tran U, Pickney LM, Ozpolat BD, Wessely O. Xenopus Bicaudal-C is required for the differentiation of the amphibian pronephros. Dev Biol. 2007; 307:152–164. [PubMed: 17521625]
44. Tran U, et al. The RNA-binding protein bicaudal C regulates polycystin 2 in the kidney by antagonizing miR-17 activity. Development. 2010; 137:1107–1116. [PubMed: 20215348]
45. Zhang B, Tran U, Wessely O. Expression of Wnt signaling components during Xenopus pronephros development. PloS one. 2011; 6:e26533. [PubMed: 22028899]
46. Xu Y, et al. The Polycystin-1, Lipoxygenase, and alpha-Toxin Domain Regulates Polycystin-1 Trafficking. J Am Soc Nephrol. 2015
47. Outeda P, et al. Polycystin signaling is required for directed endothelial cell migration and lymphatic development. Cell reports. 2014; 7:634–644. [PubMed: 24767998]
48. Coxam B, et al. Pkd1 regulates lymphatic vascular morphogenesis during development. Cell reports. 2014; 7:623–633. [PubMed: 24767999]
49. Yates LL, et al. The planar cell polarity gene Vangl2 is required for mammalian kidney-branching morphogenesis and glomerular maturation. Hum Mol Genet. 2010; 19:4663–4676. [PubMed: 20843830]
50. Lienkamp SS, et al. Vertebrate kidney tubules elongate using a planar cell polarity-dependent, rosette-based mechanism of convergent extension. Nat Genet. 2012; 44:1382–1387. [PubMed: 23143599]
51. Schneider I, et al. Zebrafish Nkd1 promotes Dvl degradation and is required for left-right patterning. Dev Biol. 2010; 348:22–33. [PubMed: 20858476]
52. Pennekamp P, et al. The ion channel Polycystin-2 is required for left-right axis determination in mice. Curr Biol. 2002; 12:938–943. [PubMed: 12062060]
53. Wu G, Somlo S. Molecular genetics and mechanism of autosomal dominant polycystic kidney disease. Mol Genet Metab. 2000; 69:1–15. [PubMed: 10655152]
54. Huang L, et al. A Possible Zebrafish Model of Polycystic Kidney Disease: Knockdown of wnt5a Causes Cysts in Zebrafish Kidneys. Journal of visualized experiments : JoVE. 2014
55. Steigelman KA, et al. Polycystin-1 is required for stereocilia structure but not for mechanotransduction in inner ear hair cells. J Neurosci. 2011; 31:12241–12250. [PubMed: 21865467]
56. Ohata S, et al. Mechanosensory Genes Pkd1 and Pkd2 Contribute to the Planar Polarization of Brain Ventricular Epithelium. J Neurosci. 2015; 35:11153–11168. [PubMed: 26245976]
57. Ohata S, et al. Loss of Dishevelleds disrupts planar polarity in ependymal motile cilia and results in hydrocephalus. Neuron. 2014; 83:558–571. [PubMed: 25043421]
58. Lu W, et al. Comparison of Pkd1-targeted mutants reveals that loss of polycystin-1 causes cystogenesis and bone defects. Hum Mol Genet. 2001; 10:2385–2396. [PubMed: 11689485]
59. Xiao Z, Zhang S, Magenheimer BS, Luo J, Quarles LD. Polycystin-1 regulates skeletogenesis through stimulation of the osteoblast-specific transcription factor RUNX2-II. J Biol Chem. 2008; 283:12624–12634. [PubMed: 18321855]
60. Kolpakova-Hart E, et al. Growth of cranial synchondroses and sutures requires polycystin-1. Dev Biol. 2008; 321:407–419. [PubMed: 18652813]
61. Karumanchi SA, et al. Cell surface glypicans are low-affinity endostatin receptors. Mol Cell. 2001; 7:811–822. [PubMed: 11336704]
62. Sive, HL.; Grainger, RM.; Harland, RM. Early Development of Xenopus Laevis: A Laboratory Manual. Vol. 395. Cold Spring Harbor Laboratory Press; New York: 2000.
63. Nieeuwkoop, PD.; Faber, J. Normal Table of Xenopus laevis (Daudin). Garland Publishing Inc; New York: 1994.
64. Xu Y, et al. The Polycystin-1, Lipoxygenase, and alpha-Toxin Domain Regulates Polycystin-1 Trafficking. J Am Soc Nephrol. 2015
65. Sheldahl LC, et al. Dishevelled activates Ca2+ flux, PKC, and CamKII in vertebrate embryos. J Cell Biol. 2003; 161:769–777. [PubMed: 12771126]

66. Vize PD, Jones EA, Pfister R. Development of the Xenopus pronephric system. Dev Biol. 1995; 171:531–540. [PubMed: 7556934]

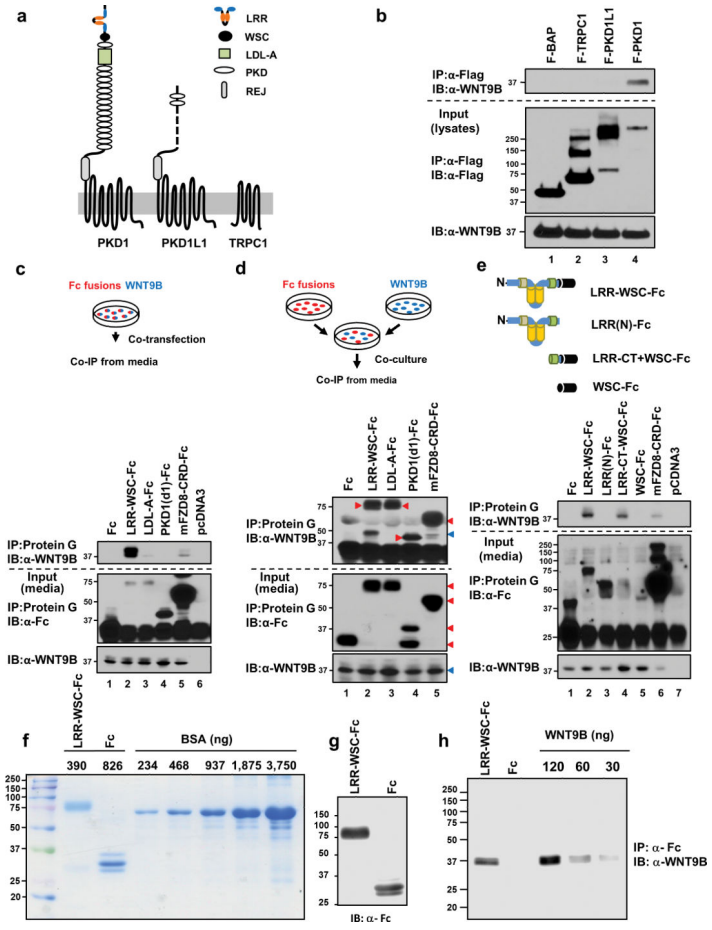

Figure 1. WNT9B binds to the extracellular domain of PKD1

(a) Membrane topology of full length PKD1, PKD1L1, and TRPC1. **(b)** Interaction of Flag-tagged PKD1 (F-PKD1), but not bacterial alkaline phosphatase (F-BAP), F-PKD1L1, or F-TRPC1 and WNT9B in lysates of transfected HEK293T cells. **(c)** Interaction of WNT9B and the LRR-WSC domain of PKD1 fused to Fc in conditioned media of co-transfected HEK293T cells. Mouse FZD8-CRD-Fc was used as positive control. **(d)** Interaction of WNT9B with the LRR-WSC domain of PKD1 fused to Fc in conditioned media *in trans* using co-cultures of HEK293T cells singly transfected with plasmids carrying Fc fusions or WNT9B. Red or blue arrow heads indicate Fc fusions or WNT9B, respectively. In upper panel, Fc fusions were non-specifically labeled (indicated by red arrow heads) by the secondary bovine α-goat used to detect α-WNT9B. **(e)** Interaction of WNT9B with a minimal domain in PKD1 containing the C-terminal cysteine rich domain of the LRR and WSC domain (LRR-CT+WSC) in conditioned media of co-transfected HEK293T cells. **(f-h)** Interaction of WNT9B with the LRR-WSC domain of PKD1 using purified proteins. **(f)** Coomassie blue staining showing the purification of LRR-WSC-Fc or Fc from the conditioned media of stably transfected HEK293 cells. **(g)** Western blotting of purified Fc fusions using α-Fc. **(h)** 390 ng of purified LRR-WSC-Fc or Fc were incubated with 500 ng/ml purified WNT9B. Fc fusions were pulled down with protein G and immunocomplexes were blotted with α-WNT9B. 87 ng of WNT9B bound to 390 ng of LRR-WSC-Fc (lane 1). 120, 60, or 30 ng of purified WNT9B were used as reference points. Experiments were

successfully repeated 2 (b,d,f,g,h) or 5 (c,e) times. Unprocessed blots are shown in Supplementary Fig. 8.

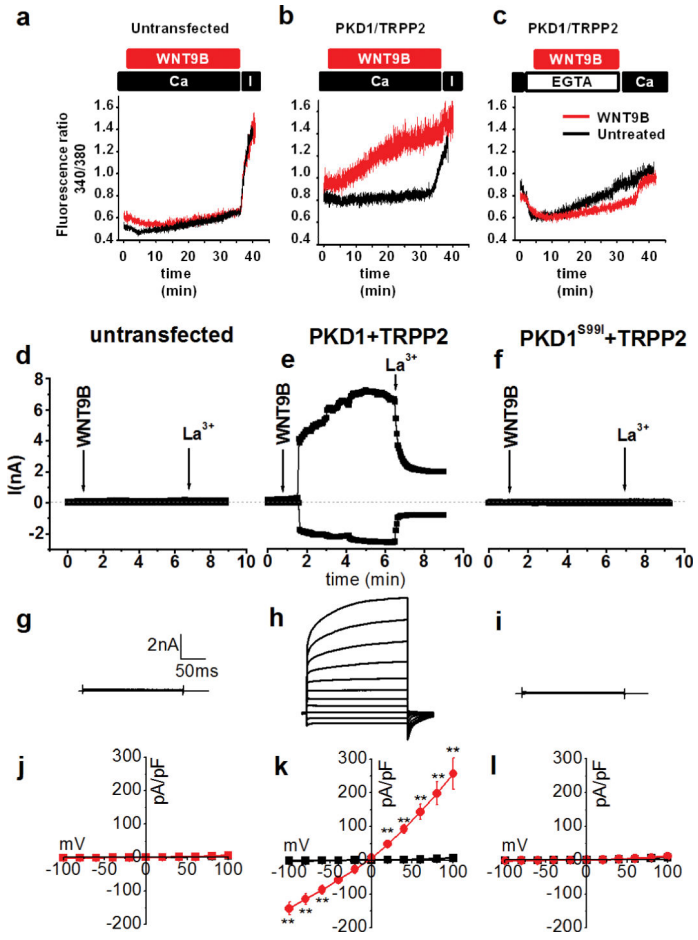

Figure 2. WNT9B activates PKD1/TRPP2

Time course of WNT9B-induced $\Delta[Ca^{2+}]_i$ (shown as fluorescence ratio 340/380) in untransfected **(a, red,** n=52 cells pooled from 3 independent experiments) or PKD1/TRPP2 co-transfected CHO-K1 cells **(b, red,** n=30 cells pooled from 5 independent experiments) in 1.8 mM extracellular Ca^{2+}. Ionomycin (I, 2 μM) was added at time point 35 min. **(c)** Time course of WNT9B-induced $\Delta[Ca^{2+}]_i$ in PKD1/TRPP2 co-transfected CHO-K1 cells (red, n=65 cells pooled from 5 independent experiments) in Ca^{2+} free extracellular solution (10 μM EGTA). $\Delta[Ca^{2+}]_i$ in PBS-treated cells in all three conditions is shown in black. **(d-l)** Time course (d-f), step currents **(g-i)**, or I-V curves of WNT9B (500 ng/ml)-induced whole cell currents in untransfected **(d,g,j)**, PKD1/TRPP2 co-transfected **(e,h,k)** or $PKD1^{S99I}$/TRPP2-co-transfected CHO-K1 cells **(f,i,l)** in 50 nM intracellular Ca^{2+} concentration. La^{3+} (100 μM) was added at the indicated times. I-V curves were taken before (black) and 5 min after (red) the addition of WNT9B in the bath solution of untransfected **(j,** n=6 cells pooled from 2 independent experiments), PKD1/TRPP2- **(k,** n=12 cells pooled from 4 independent experiments), or $PKD1^{S99I}$/TRPP2-co-transfected CHO-K1 cells **(l,** n=6 cells pooled from 4 independent experiments). Representative time courses (d-f) and step currents (g-i) from 6 (untransfected), 12 (PKD1+TRPP2), or 6 ($PKD1^{S99I}$+TRPP2) cells. All statistical tests were performed using paired Student's t-test, $^{**}P<0.01$. Data are shown as mean ± SEM.

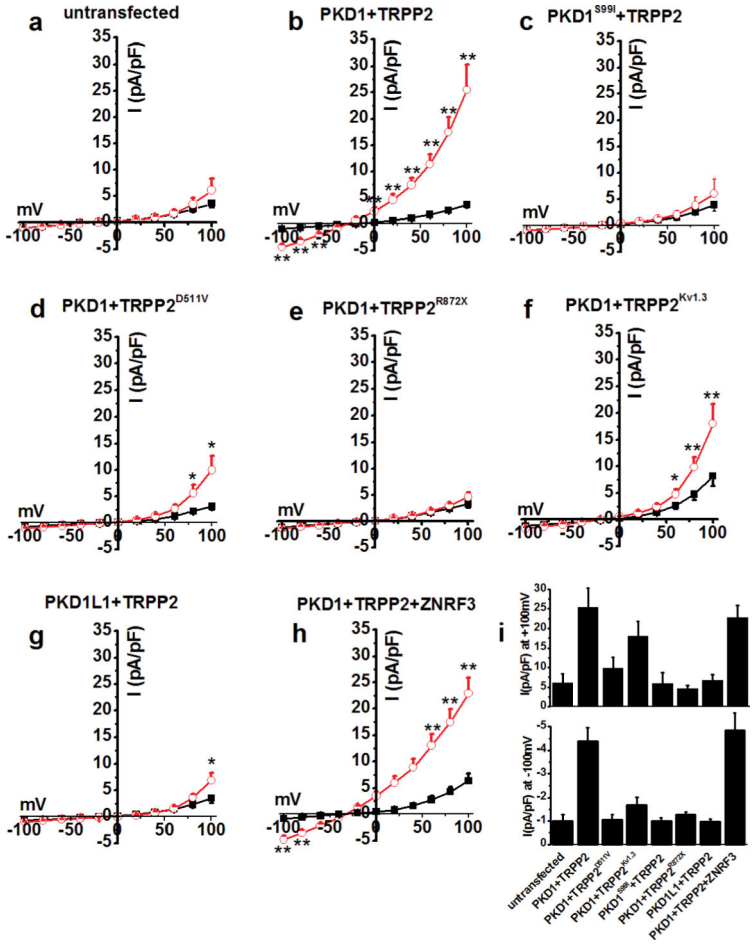

Figure 3. Pathogenic mutations in PKD1 or TRPP2 suppress activation by WNT9B

(a-h) I-V curves taken before (black) and 5 min after the addition of WNT9B (500 ng/ml) in the bath solution (red) of untransfected **(a,** n=5 cells pooled from 2 independent experiments), PKD1/TRPP2- **(b,** n=8 cells from 3 independent experiments), or PKD1^{S99I}/TRPP2- **(c,** n=7 cells from 3 independent experiments), PKD1/TRPP2^{D511V}- **(d,** n=11 from 4 independent experiments), PKD1/TRPP2^{R872X}- **(e,** n=7 cells from 3 independent experiments), PKD1/TRPP2$^{Kv1.3}$- **(f,** n=12 cells from 5 independent transfections), PKD1L1/TRPP2- **(g,** n=9 cells from 5 independent experiments), or PKD1/TRPP2/ZNRF3- **(h,** n=11 cells pooled from 3 independent transfections) co-transfected CHO-K1 cells in zero intracellular Ca^{2+}. **(i)** Summary data of inward (−100 mV) or outward currents (+100 mV) from all groups. Differences between current densities before and after WNT9B for any given membrane potential in I-V curves were determined using paired Student's t-test, *P<0.05, **P<0.01. Data are shown as mean ± SEM.

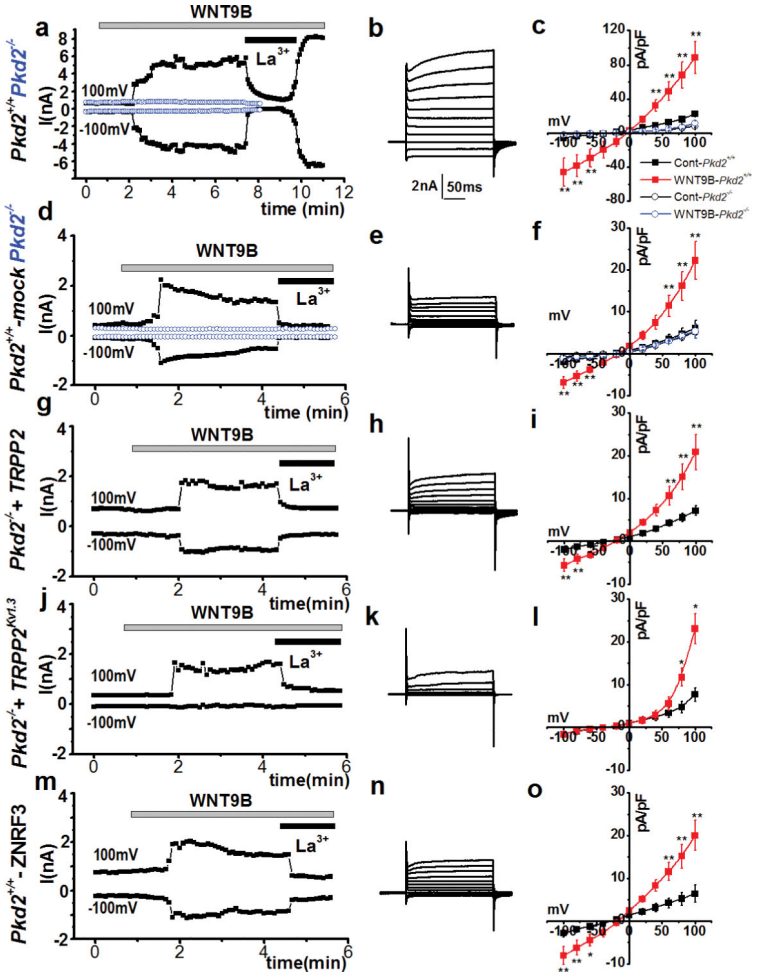

Figure 4. TRPP2 mediates WNT9B-induced whole cell currents in MEFs

(a-c) Time course **(a)**, step currents **(b)**, and I-V curves of WNT9B-induced whole cell currents in 50 nM intracellular Ca^{2+} **(c,** n=7 cells pooled from 3 independent experiments), before (Cont-*Pkd2*$^{+/+}$) or after WNT9B (500 ng/ml, WNT9B-*Pkd2*$^{+/+}$) in wild type *Pkd2*$^{+/+}$ MEFs. Time course of WNT9B-induced currents in *Pkd2*$^{-/-}$ MEFs is shown as open blue circles in (a), whereas I-V curves are shown as open black (Cont-*Pkd2*$^{-/-}$) and open blue circles (WNT9B-*Pkd2*$^{-/-}$) in (c) (n=6 cells from 3 independent experiments). **(d-l)** Time course, step currents, and I-V curves of WNT9B-induced whole cell currents in zero intracellular Ca^{2+} in mock- transfected (just CD8α) **(d-f,** n=6 cells from 3 independent experiments), wild type TRPP2- transfected **(g-i**, n=12 cells from 5 experiments), or $TRPP2^{Kv1.3}$- transfected *Pkd2*$^{-/-}$ cells **(j-l**, n=5 cells pooled from 3 independent experiments). Time course and I-V curves of WNT9B-induced currents in zero intracellular Ca^{2+} in *Pkd2*$^{-/-}$ cells is shown as open blue circles in (d) and (f, n=6 cells pooled from 3 independent experiments). **(m-o)** Time course, step currents, and I-V curves of WNT9B-induced whole cell currents in zero intracellular Ca^{2+} in ZNRF3-transfected *Pkd2*$^{+/+}$ MEFs (n=12 cells pooled from 4 independent experiments). Step currents are shown 5 min after the addition of WNT9B (500 ng/ml) in the bath solution. I-V curves were taken before (black) and 5 min after the addition of WNT9B (red). Differences between current densities before

and after WNT9B for any given membrane potential in I-V curves were determined using paired Student's t-test, *P<0.05, **P<0.01. Data are shown as mean ± SEM. Representative images of time courses (a,d,g,j,m) and step currents (b,e,h,k,n) were obtained from 7, 6, 12, 5, 12 cells, respectively.

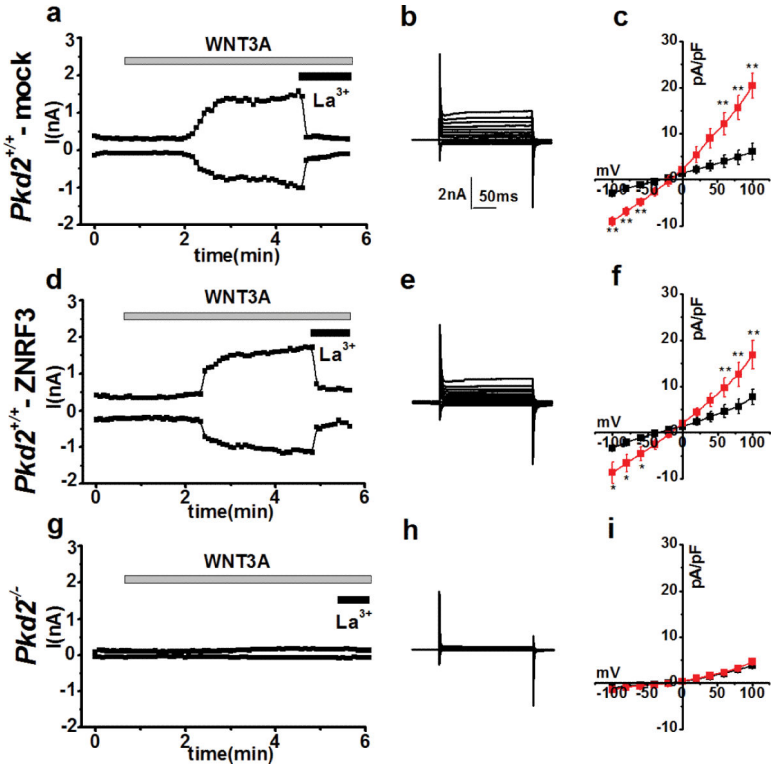

Figure 5. TRPP2 mediates WNT3A-induced whole cell currents in MEFs

Time course, step currents, and I-V curves of WNT3A-induced whole cell currents in zero intracellular Ca^{2+} in mock- **(a-c,** n=16 cells pooled from 6 independent experiments), or ZNRF3-transfected *Pkd2*$^{+/+}$ **(d-f**, n=20 cells pooled from 7 independent experiments) or *Pkd2*$^{-/-}$ MEFs **(g-i,** n=9 cells from 4 independent experiments) before (black) and after the addition of WNT3A (500 ng/ml) in the bath solution (red). Step currents are shown at 5 min after the addition of WNT9B in the bat solution. Statistical analysis was performed using paired Student's t-test, **P*<0.05, ***P*<0.01. Data are shown as mean ± SEM. Representative images of time courses (a,d,g) and step currents (b,e,h) were obtained from 16, 20, 9 cells, respectively.

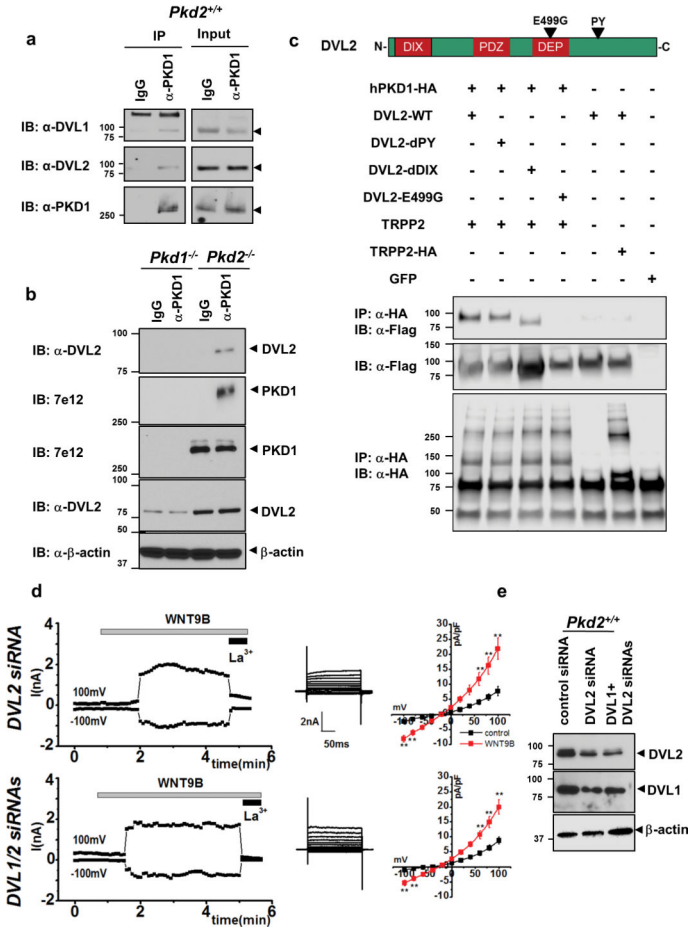

Figure 6. Interaction of DVL1 and DVL2 with PKD1 in MEFs and transiently transfecte HEK293T cells

(a) Wild type MEF cell lysates were incubated with mouse IgG1 control antibody or mouse monoclonal α-PKD1 (E4). Immunocomplexes were immunoblotted with rabbit polyclonal α-DVL1 (upper left panel), α-DVL2 (middle left panel), or mouse monoclonal α-PKD1 (7e12, lower left panel). Expression levels of DVL1, DVL2, or PKD1 in lysates incubated with mouse IgG1 control or α-PKD1 (E4) are shown in right panels (input). Experiments were successfully repeated 3 times. **(b)** Cell lysates from *Pkd1*$^{-/-}$ or *Pkd2*$^{-/-}$ MEFs were incubated with mouse IgG1 control antibody or mouse monoclonal α-PKD1 (E4) and DVL2 was detected in the immunocomplexes, as described in (a). Experiments were successfully repeated twice. **(c)** HEK293T cells were transiently transfected with indicated plasmids and PKD1 or TRPP2 was pulled down with α-HA. Flag-tagged wild type or mutant DVL2 was detected using α-Flag. DIX (DIshevelled and aXin), PDZ, or DEP (Dishevelled, Egl-10 and Plecstrin) domains are shown red in DVL2 diagram. Position of E499G mutation and PY motif are shown by a black arrow head. Experiments were successfully repeated 3 times. **(d)** Time course, step currents and I-V curves in zero intracellular Ca^{2+} of wild type MEFs transiently transfected with a DVL2-specific siRNA (n=18 cells pooled from 5 independent experiments) or a mixture of DVL1 and DVL2 siRNAs (n=13 cells pooled from 4 independent experiments). Statistical tests were performed using paired Student's t-test, $^{**}P<0.01$. Data are shown as mean ± SEM. **(e)** Knockdown efficiency of DVL1 and DVL2

siRNAs. Wild type MEFs were transiently transfected with indicated siRNAs and cell lysates were immunoblotted with α-DVL1, α-DVL2, or α-β-actin. Experiment was done once. Unprocessed original scans of blots are shown in Supplementary Fig. 8).

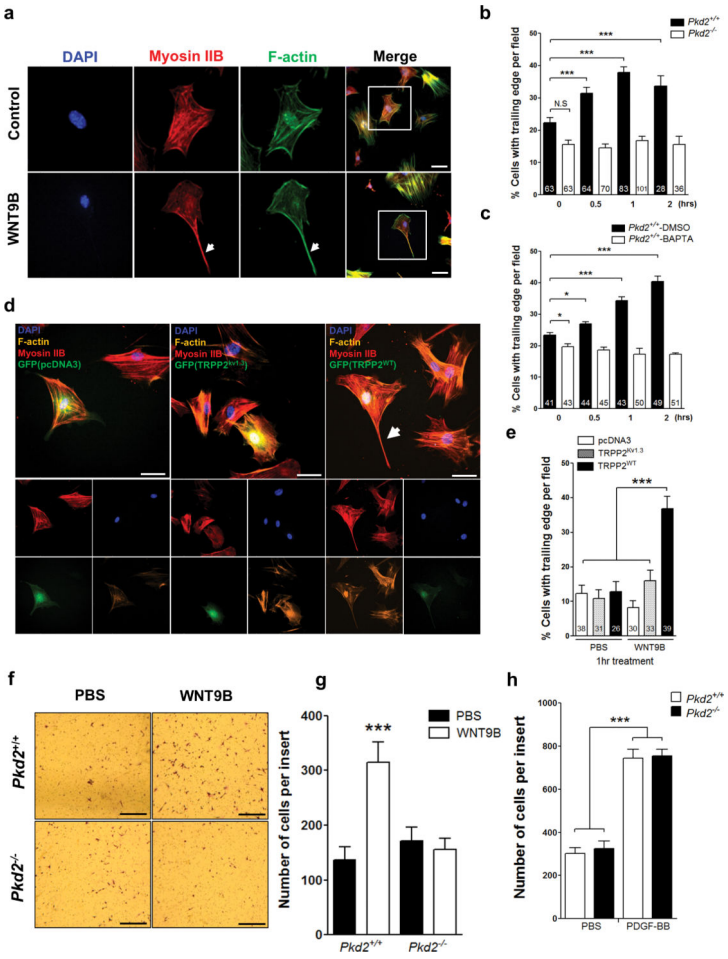

Figure 7. TRPP2 mediates WNT9B-induced cell migration

(a) *Pkd2*$^{+/+}$ cells stained with phalloidin (green, to visualize F-actin), Myosin IIB (red), or DAPI (blue) at 0 (Control) or 30 min after the addition of WNT9B (500 ng/ml). Arrow heads indicate accumulation of F-actin and Myosin IIB in the trailing edge of a migrating cell. Scale bar, 50 μm. **(b)** Percentage of *Pkd2*$^{+/+}$ cells with trailing edge per field (total number of fields of cells pooled from 3 independent experiments shown in graph) incubated with WNT9B or PBS at different time points. **(c)** Percentage of cells with trailing edge per field (total number of fields of cells pooled from 3 independent experiments shown in graph) in *Pkd2*$^{+/+}$ MEFs incubated with WNT9B in the presence or absence (DMSO) of 10 μM BAPTA/AM at different time points. **(d)** Representative images of GFP-, GFP+TRPP2^{WT}- or GFP+TRPP2$^{Kv1.3}$-transfected *Pkd2*$^{-/-}$ cells stained for F-actin (yellow) and Myosin IIB (red). Scale bar, 50 μm. **(e)** Percent of migrating GFP-positive cells in three groups treated for 1 h with PBS or WNT9B (500 ng/ml) from one representative out of three independent transfections (total number of fields of cells from a single experiment, that was independently repeated three times are shown in graph). Statistics source data for all three experiments are available in **Suppl. Table 3**. **(f)** Cells migrated through a trans-well filter in the presence of WNT9B (1 μg/ml) or PBS for 6 h. Scale bar, 500 μm. **(g)** Number of migrating *Pkd2*$^{+/+}$ or *Pkd2*$^{-/-}$ cells through a trans-well filter in the presence of PBS or WNT9B. n= 18 fields per group pooled from 3 independent experiments scoring a total of

2462 (*Pkd2*$^{+/+}$-PBS), 5665 (*Pkd2*$^{+/+}$-WNT9B), 3091 (*Pkd2*$^{-/-}$-PBS), or 2796 (*Pkd2*$^{-/-}$-WNT9B) cells. **(h)** Number of migrating cells in the presence of PBS or PDGF-BB (25 ng/ml). Data were pooled from 3 independent experiments in quadruplicates (n= 12 fields per group scoring a total of 3625 (*Pkd2*$^{+/+}$-PBS), 8927 (*Pkd2*$^{+/+}$-PDGF-BB), 3904 (*Pkd2*$^{-/-}$-PBS), or 9048 (*Pkd2*$^{-/-}$-PDGF-BB) cells. N.S means non-significant, *P<0.05, ***P<0.001 in one-way ANOVA followed by Neuman-Keuls *post hoc* test. Data are shown as mean ± SEM.

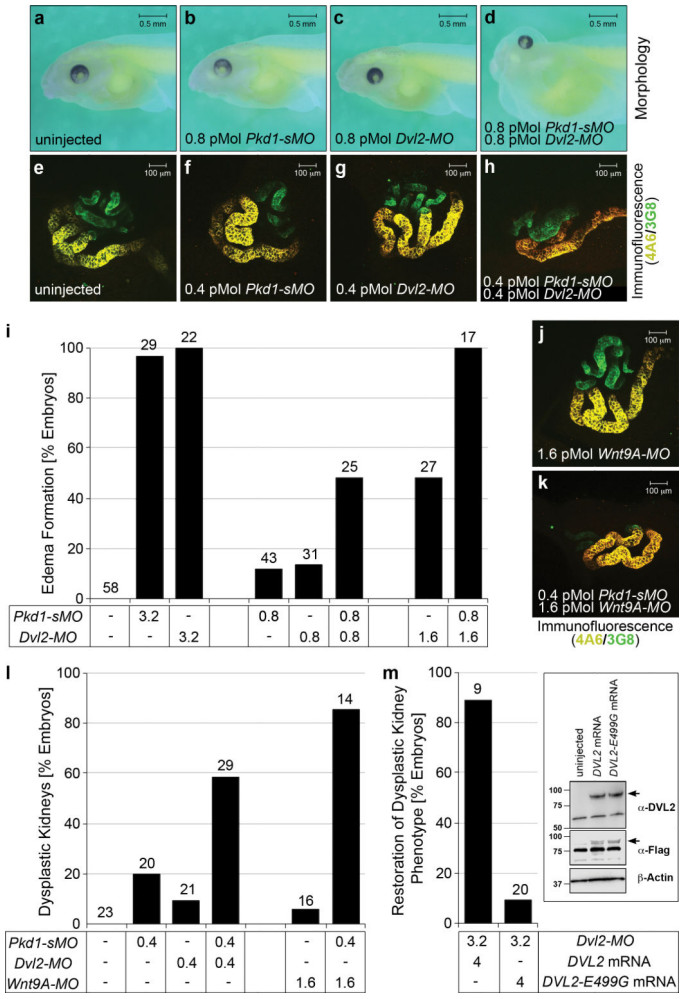

Figure 8. Cooperativity between PKD1 and DVL2 in *Xenopus*

(a-l) *Xenopus* embryos were injected with the indicated amounts of *Pkd1-sMO1, Dvl2-MO* and *Wnt9A-MO* either alone or in combination. Embryos were analyzed at stage 43 by morphology for edema formation or at stage 40 by immunofluorescence with the proximal tubular marker 3G8 (green) and the distal tubule/nephric duct marker 4A6 (yellow). Representative images of an uninjected control **(a,e)** and embryos injected with suboptimal amounts of *Pkd1-sMO1* **(b,f)**, *Dvl2-MO* **(c,g),** a mixture of *Pkd1-sMO1* and *Dvl2-MO* **(d,h)**, as well as with a *Wnt9A-sMO* alone **(j)** or in combination with suboptimal amounts of *Pkd1-sMO1* **(k)** are shown. Bar diagrams showing the percentage of embryos exhibiting edema or dysplastic kidneys from 4 or 3 independent experiments are shown in **(i)** or **(l)**, respectively. **(m)** Rescue experiment of *Dvl2* morphants with a unilateral injection of either 4 ng wild type human *DVL2* mRNA or 4 ng mutant *DVL2-E499G* mRNA. Embryos were analyzed at stage 40 by 3G8/4A6 immunofluorescence comparing the mRNA injected side with the contralateral side. Bar diagram depicts the summary of 3 independent experiments. (Inset) Expression levels of Flag-tagged human DVL2 and DVL2-E499G mutant in stage 25 embryos injected with 1 ng mRNA into a single blastomere at the 4-8 cell stage. Experiment was done twice. Total number of scored embryos is shown on top of each bar.